A novel neutron texture diffractometer analyzing method with Convolutional Neural Networks for Face-Centered Cubic Material*

Bokai Zhao,[1] Weimin Gan,[2] Danmin Liu,[3] Xiaolong Liu,[1] Yuhan Hou,[1] Yuqing Li,[1] Tianfu Li,[1] Kai Sun,[1] Xueshen Jiao,[1] Meijuan Li,[1,†] Dongfeng Chen,[1,‡] and Yingxun Zhang[1,§]

[1]*Department of Nuclear Physics, China Institute of Atomic Energy, Beijing 102413, China*
[2]*GEMS at MLZ, Helmholtz - Zentrum Hereon D-85748, Garching, Germany*
[3]*Institute of Microstructure and Properties of Advanced Material, Beijing University of Technology, Beijing 100124, China*

In this study, we propose a convolutional neural network (CNN) model aimed at inferring texture types and their volume fractions from neutron diffractometer data. The model is trained using labeled texture data of face-centered cubic (FCC) materials, primarily sourced from X-ray diffraction (XRD) measurements. The effectiveness of the model is evaluated using data obtained from neutron diffraction. Compared to traditional data analysis methods, the CNN model not only offers faster and more accurate predictions of texture components and their volume fractions, but also demonstrates strong generalization ability. Even under a certain signal-to-noise ratio, the CNN model maintains high accuracy in inferring texture types and their volume fractions. This capability could facilitate the operation of neutron texture diffractometers at lower neutron beam intensities in the future, thus improving both the efficiency and precision of texture analysis.

Keywords: convolutional neural networks, texture, neutron diffraction, X-ray diffraction, face-centered cubic material

The crystallographic texture, which refers to the preferred orientation distribution of grains within polycrystalline materials, can lead to anisotropy of material properties [1–3] and thus influence both the processing behavior and the service performance of materials. Additionally, texture is a key factor in material failure mechanisms [4]. As such, accurate characterization and analysis of texture are essential for guiding texture control, optimizing processing conditions, and enhancing the overall performance of materials. Techniques such as electron backscatter diffraction (EBSD), X-ray diffraction (XRD), and neutron diffraction (NuD) offer complementary approaches for the characterization of crystallographic texture in polycrystalline materials [5–7]

The texture measurement of polycrystalline material usually requires the collection of diffraction data from hundreds to thousands of orientation positions. The use of two-dimensional position sensitive detector has improved the measurement efficiency of neutron texture diffractometer[8], which means that more data needs to be collected in a short period of time. As a result, two main challenges arise in texture data processing. First, the collection of a large number of data slows down the processing speed and impedes real-time assessment of the texture information of the measured materials. This is because the texture data processing involves multiple steps, including data acquisition, pre-processing, diffraction peak fitting, normalization, and pole figure construction to derive the pole figure data [9]. Second, the accuracy of the current texture analysis methods is often compromised by significant errors in diffraction peak intensity fitting, particularly for polycrystalline materials that exhibit weak overall texture, a combination of strong and weak texture components, or strongly overlapping diffraction peaks.

To improve the efficiency and accuracy of texture data analysis, a state-of-the-art machine learning (ML) method may be useful. The reason is that the ML method can be used to construct a direct mapping relationship between the pole figures and the final results on the texture information after the training. Thus, the texture information can be obtained directly from the original pole figure data, and it will save a lot of time. In addition, due to the strong identification ability of machine learning for weak signals, it is possible to achieve more accurate analysis of weak texture components, which improves the accuracy of data analysis. Therefore, the ML method has attracted the attention of scientists from the neutron scattering laboratory in recent years on the different fields or instruments, such as single crystal neutron diffractometer[10], macromolecular neutron diffractometer[11], neutron reflectometer[12, 13], neutron residual stress diffractometer[14], neutron small angle spectrometer[15, 16] and neutron imaging facility[17]. However, the application of ML in texture data analysis has not been reported.

In this paper, we propose an ML method in texture data analysis. The initial step is to extend the pole figure data obtained through XRD to the same angle range as the pole figure data obtained through NuD by linear interpolation, which forms a data set that can be used to train the model. Then the model is trained from the data set using CNN. Finally, the model is used to predict the texture components and volume fraction of the FCC structure material measured by NuD.

Now, let's show how we prepare the training data set $D = \{D_1, \cdots, D_N\}$. The data set D_i is composed of the measured pole figure data of FCC structural materials on three

* Supported by the National Natural Science Foundation of China (Grant 12275359), China National Nuclear Corporation (Grant FY222506000101), National Natural Science Foundation of China (Grant 12075321), Continuous Basic Scientific Research Project (16BJ010261224864) and Director's Foundation of China Institute of Atomic Energy(16YZ010270324221). The authors thank Prof. Chun-Wang Ma's helpful suggestions.

† Corresponding author, mjli@ciae.ac.cn
‡ Corresponding author, dongfeng@ciae.ac.cn
§ Corresponding author, zhyx@ciae.ac.cn

crystal planes, such as, (111), (200), and (220) crystal planes, and the corresponding volume fraction of the texture component V_{frac}. That is $D_i = (I(\chi,\phi), V_{frac})_i$, and $I(\chi,\phi) = (I_{(111)}(\chi,\phi), I_{(200)}(\chi,\phi), I_{(220)}(\chi,\phi))$. $I_{(hkl)}(\chi,\phi)$ is the intensity of signal of crystal plane (hkl) at χ angle and ϕ angle, V_{frac} is the volume fractions of the six most representative texture components of the face-centered cubic structure. Totally, we have 178 sets of the pole figure data, 121 sets of them were measured by XRD and 16 sets of them were measured by NuD.

More details, both XRD and NuD measurements use an equal angle χ and ϕ interval measurement method with a step size of $5° \times 5°$ as shown in Fig. 1, and provide the intensity of signal $I_{(hkl)}(\chi,\phi)$. Then LaboTex software was used to analyze the collected data, and the volume fractions of the six most representative texture components of the face-centered cubic structure, i.e. V_{frac}, were recorded as labels and calculated: Goss component, Brass component, Cube component, Copper component, S component and R component.

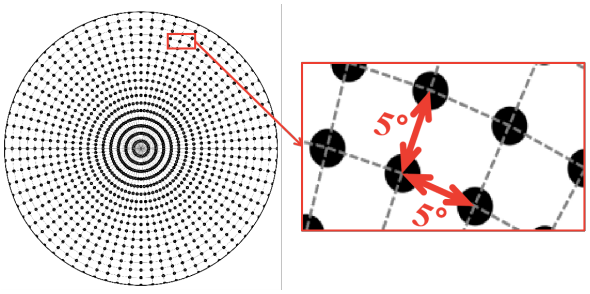

Fig. 1. Distribution of sampling points measured at equal angle intervals.

To solely determine the texture in face-centered cubic structure materials, normally pole figures from 3 different crystal planes must be measured. Thus, the feature of the data set composed of XRD measurements is an incomplete matrix of $3 \times 14 \times 72$ size, i.e., $(I_{(111)}(\chi,\phi), I_{(200)}(\chi,\phi), I_{(220)}(\chi,\phi))$. Here, 3 means three different crystal planes, 14 and 72 mean the number of intervals in χ and ϕ angle. The NuD measurement can obtain a complete pole figure, and its sample feature is a three-dimensional matrix of $3 \times 19 \times 72$ size. Considering that the our main use scene of the model is to predict the data from the neutron texture diffractometer, we first use linear interpolation to expand the pole figure data obtained through XRD to match the angle range of the pole figure data measured by NuD, that is, the data are processed into a matrix of $3 \times 19 \times 72$ size. Then the volume fractions of the six texture components are calculated, and then used as the label of the data set.

Due to the good symmetry of the cube shaped samples, the pole figures in the (111), (220) and (222) planes show mirror symmetry with the transverse direction (TD) and rolling direction (RD) as the symmetry axis. Thus, only 1/4 of the pole figure is useful for determining the texture in material, and which means the effective data matrix will be $3 \times 19 \times 18$. However, the experimental results on the pole figure are not strictly satisfy this symmetry requirement due to the statistics

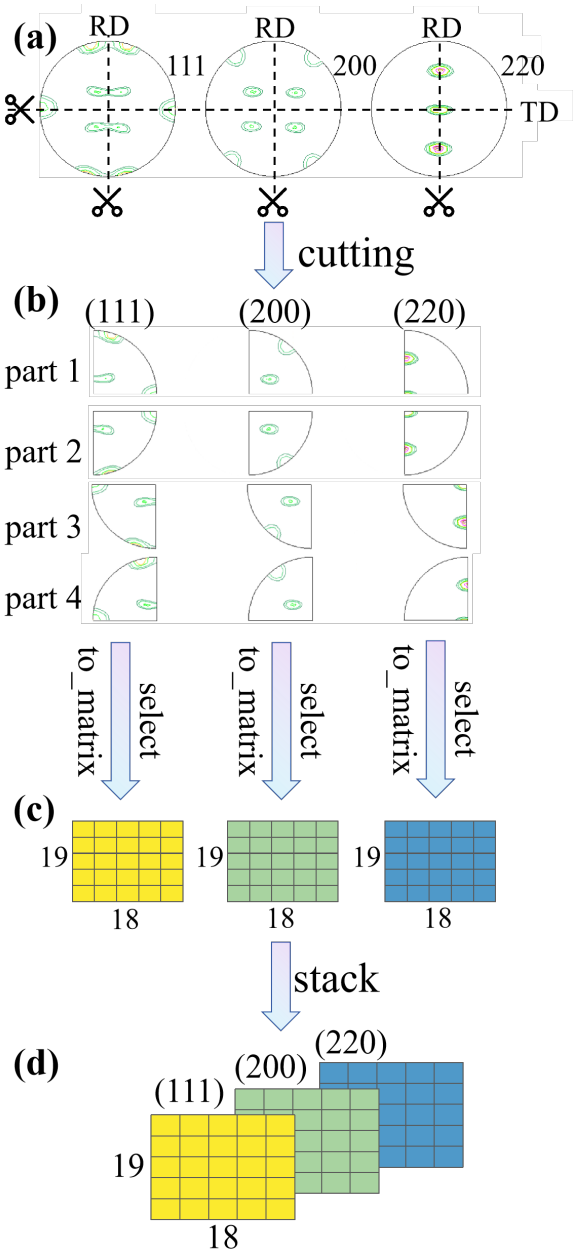

Fig. 2. Extending the number of samples in the data set by using the mirror symmetry of the polar figure.

uncertainties in the measurements. By using this statistics uncertainties and symmetry properties, we can increase the number of training data sets as the following process.

First, each measured pole figure for crystal planes are divided into four parts according to the symmetry axis as Fig. 2(a), which means we will have 12 effective pole figures. Then, we randomly select a part from one of the pole figures and convert the data of the selected part into a 19×18 matrix format. The similar selections are done for other two pole figures. Finally, the three selected matrices are stacked to form a pole figure represented by a three-dimensional matrix format, i.e., $3 \times 19 \times 18$. The advantages of our data

preparing procedure is that it can greatly increase the number of sets, that is, the data of a material can form 64 sets. On the other hand, the original matrix of $3 \times 19 \times 72$ size is reduced to $3 \times 19 \times 18$ size, which reduces the amount of calculation required to train the CNN later.

In order to facilitate the validation of the model's pattern learning ability and generalization ability in the process of training the model, the extended data set has been divided into a training set and a test set according to a ratio of 8:2. The model parameters are updated according to the training set during the learning process. The test set is employed to assess the model's predictive capacity in the new data set, and it is not involved in the learning process.

Second, the data has to be preprocessed before training the CNN model due to the following two reasons. One is that the differences in the physical properties of X-rays and neutron rays result in a considerable intensity range, from 10^2 to 10^5, as observed in the pole figure data obtained from various material tests. In order to ensure that the data set formed by XRD test results is also effective in the NuD prediction task, the measurement intensity of the sample is normalized in accordance with the following steps:

$$x(\chi,\phi) = \frac{I(\chi,\phi) - I_{min}(\chi,\phi)}{I_{max}(\chi,\phi) - I_{min}(\chi,\phi)}, \tag{1}$$

where x is the reduced measured signal intensity. $I_{min}(\chi,\phi)$ and $I_{max}(\chi,\phi)$ are the minimum and maximum measured signal intensity, respectively.

The other is that there is also a large difference on the values of the volume fraction V_{frac} among the different labels. For example, the difference between the largest value and the smallest value for the different labels reaches about 5.58, which reduce the ability of the distinguishing of the different labels. To enhance resolution, the logarithmic mapping method is employed, which is expressed as:

$$y = \ln(V_{frac} + 1). \tag{2}$$

As illustrated in Fig. 3, this nonlinear mapping is capable of suppressing considerable distinctions between volume fraction values while simultaneously preserving subtle differences between such values. Once the trained CNN model has been employed to calculate the normalized pole figure data, the predicted value can be utilized to ascertain the volume fraction of the texture in material through the application of the formula $V_{frac} = e^y - 1$.

The input for the CNN model is the features of the samples in the data set, i.e., $I(\chi,\phi)$, and CNN can effectively extract features. Mathematically, it can be simply written as,

$$V_{frac}^{CNN} = f\Big((I * \theta)(\chi,\phi)\Big). \tag{3}$$

The symbol $*$ means the convolution production between the input I and network parameter θ. f is a function obtained by CNN model. Generally, the structure of CNN is divided into feature extraction layer and fully connected layer. The feature extraction layer is composed of convolution layer, activation layer and other structures, which is used to extract

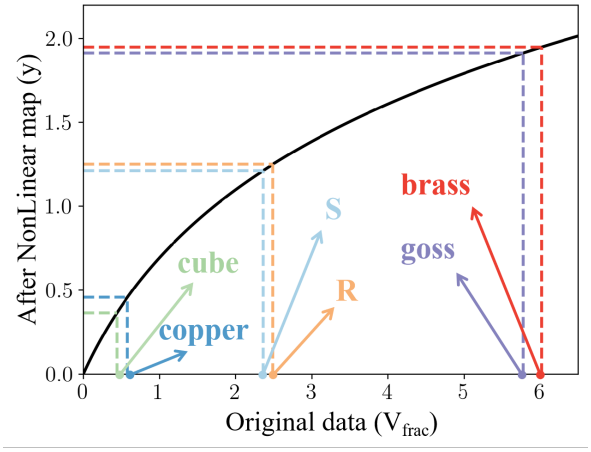

Fig. 3. The function of nonlinear mapping in the label original data space. The original data increases with a step size of 1, and the amount of data increase after nonlinear mapping becomes smaller and smaller, which can weaken the impact of large offset data.

feature information from the three-dimensional tensor. The fully connected layer can be regarded as performing prediction tasks based on the extracted features. In this paper, the CNN model, designed for the purpose of multi-task prediction, was employed for the modelling of our texture data using PyTorch[18]. An overview of the CNN structure is provided in Fig. 4 and details of the substructure of network structure are presented in Appendix A.

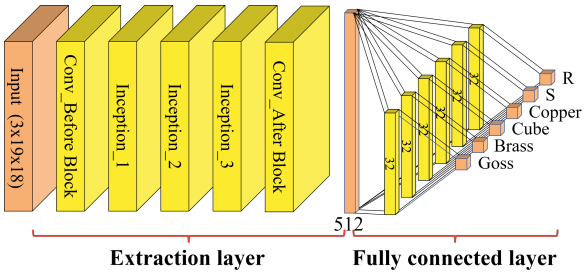

Fig. 4. Convolutional neural network structure.

The loss function L used in the CNN model for predicting the volume fraction of the six texture components is defined as,

$$L = \frac{1}{N_t}\sum_{j=1}^{N_t} MSE_j, \tag{4}$$

Here, N_t is the number of texture components and MSE_j is the mean square error for jth texture component. In this work, $N_t = 6$. The MSE_j reads,

$$MSE_j = \frac{1}{N_j}\sum_{i=1}^{N_j}\left(V_{frac,j}(i) - V_{frac,j}^{CNN}(i)\right)^2. \tag{5}$$

N_j is the number of samples for jth texture component, which equal 178*0.8=142. During the training, the stochastic gradient descent (SGD) algorithm is used.

In Fig. 5, the loss function values of the training set and the test set change during the model training process are presented by using the parameter training strategy as in Appendix B. It can be seen that the loss function value can converge to 0.00625 after about 100 epoches. The MSE as a function for each texture component is also presented in Appendix B.

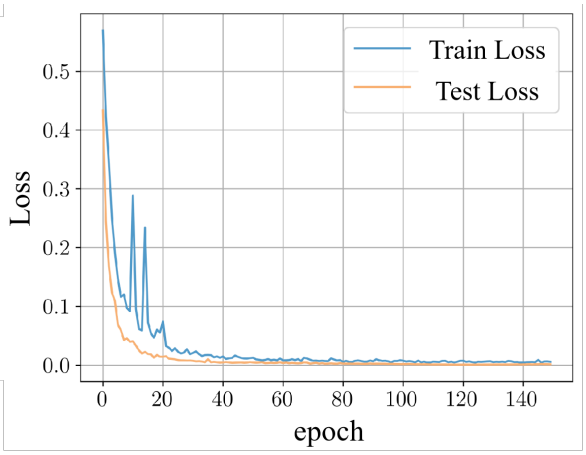

Fig. 5. Loss function value as a function of epoch for the training set and the validation set.

As we known that 88% of the training data are from the XRD measurements, 8:2 ratio between the training data and testing data could lead that the training data is completely composed from XRD. It raise an interesting issue whether the trained data only from XRD can also predict the NuD data. To demonstrate the ability of the model to predict the volume fraction of textures in the materials measured by neutron diffraction, 16 sets of data from neutron diffraction measurements are used to valid the trained model.

Firstly, we calculated the MSE_j between the predicted results and the true values of each texture component. Generally speaking, MSE is a indicator to measure the prediction accuracy of the model. When the value of MSE is closer to 0, it means that the prediction performance of the model is good. However, the definition of MSE with Eq.(5) could also lead a smaller value when the absolute value of V_{frac} is small. To avoid this misunderstanding, $R2$ is an alternative choice which is usually used to reflect the goodness of fitting. The definition of $R2$ is,

$$R2 = 1 - \frac{\sum_{i=1}^{N}\left(V_{frac}^{CNN}(i) - V_{frac}(i)\right)^2}{\sum_{i=1}^{N}\left(\overline{V_{frac}^{CNN}}(i) - V_{frac}(i)\right)^2}. \quad (6)$$

Here, $\overline{V_{frac}^{CNN}}(i)$ is the average value of the predicted result. If the prediction can well reproduce the true data, the value of R2 is closer to 1. The calculation results for both MSE and R2 are shown in Fig. 6, in which the mean square error index of brass texture is the largest, but the value is only 0.03891. The lowest index of goodness of fit is 0.98805. This shows that the model can well predict the volume fraction of a certain texture on the data of neutron diffraction measurement.

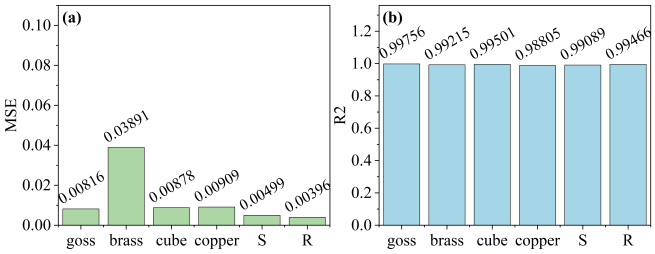

Fig. 6. The MSE and R2 indicators of the model prediction ability on the data set of neutron diffraction measurement material texture.

To deeply understand the goodness of the CNN model prediction on the volume fraction of the six texture components, it will be interesting to check the distributions of the absolution error, i.e., $P(\Delta V_{frac})$, of the test data sets by using quartiles. Here, $\Delta V_{frac} = |V_{frac}(i) - V_{frac}^{CNN}(i)|$. The squares in the box represent the mean of the ΔV_{frac}. As shown in Fig. 7, the model can accurately predict the volume fraction of the six texture components simultaneously, with the average absolute error of less than 0.38% and the maximum absolute error of 0.52%.

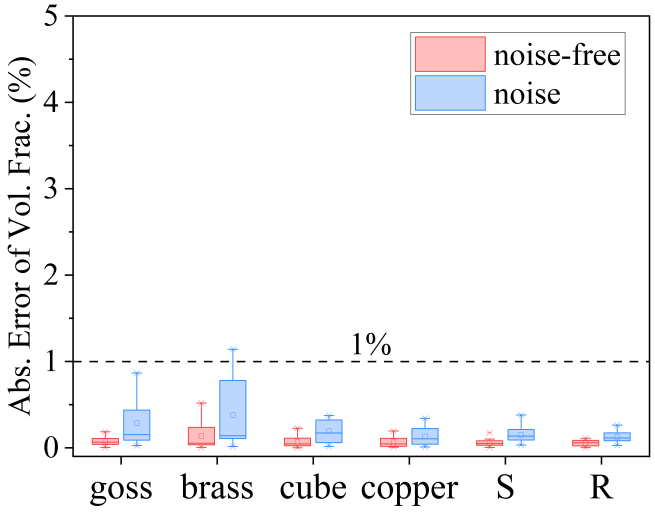

Fig. 7. Absolute error distributions in the case of noise-free and noise.

Finally, in order to verify that the CNN can still predict the data accurately even under small signal-to-noise ratio, we add a randomly noise signal to the measured data. The intensity of the noise signal is set as 10% of the maximum signal intensity measured in the experiment. The results are also displayed in Fig. 7 quartiles which are presented as blue boxes and vertical lines. Our results show that the maximum absolute error of 0.8% except for the brass texture component. Even for brass texture, 75% of absolute error points are less than 0.8%. This quartile figure evidence that the prediction using CNN retains the good anti-interference ability.

In summary, we present the construction of a CNN that is suitable for multi-objective prediction from pole figure data obtained by XRD measurements of face-centered cubic materials. The model was trained using the SGD algorithm and subsequently tested on pole figure data obtained from neutron diffraction measurements. The analysis results demonstrate that the model retains a high degree of predictive capability on the neutron diffraction measurement data, even though the fact that the dataset originates from XRD measurements. This is attributed to latent parameters learned in the CNN model containing the correct texture component information, which makes the CNN model arrive at the correction conclusion on the texture component whatever the input data from XRD or NuD.

Furthermore, the application of the CNN model to analyze pole figure data not only enables the rapid prediction of material texture information but also exhibits considerable potential for utilization in specific scenarios. For example, the robust data anti-interference capacity of deep neural networks enables the delivery of more precise texture information in complex scenarios, such as neutron in-situ texture measurement.

Appendix A: Details of CNN structure

The feature extraction layer in CNN is divided into five parts, and the specific structure of each part is shown in Fig. 8. In the feature extraction layer, Batch Norm[19] and ReLU activation operations are performed on all convolution blocks, as shown in Fig. 8(a). To make it easier to design the CNN structure, the matrix size is expanded to a square matrix by 0-filling, and then computed according to the structure shown in Fig. 8(b). The data is then passed through three different parallel computing modules of Inception. These modules are the same as the Inception module structure of GoogLeNet[20], and their structure is shown in Fig. 8(c)-(e). Finally, the structure shown in Fig. 8(f) is used to further extract features, resulting in 512 features. These features extracted from the feature extraction layer are fed into six fully connected layers with identical structure but no common parameters. Unlike the ReLU activation function used in the feature extraction layer, the activation function used in the fully connected layer is Tanh[21] to improve the nonlinear mapping ability of the data. These layers are used to predict the volume fraction of the corresponding texture components.

Appendix B: Details of CNN training and validation

In this network structure, the algorithm used to update the neural network parameters is stochastic gradient descent (SGD), and the corresponding parameter update strategy is:

$$\theta_{new} = \theta_{old} - l_r \frac{\partial L}{\partial \theta}, \tag{B1}$$

where l_r is the learning rate. L is the loss function, and the formulas are Eq.(4) and Eq.(5).

In order to make the model have good predictive ability, the learning rate needs to be set as small as possible. However, the smaller learning rate is easy to make the model fall into the local minimum value, so we use the CyclicLR learning rate scheduling strategy[22]. The strategy's feature is the learning rate shows a periodic attenuation change with the increase of the number of iterations. The learning rate used here ranges from 0.00003 to 0.003. One cycle contains 120 iterations, the maximum learning rate in each cycle is half of the previous cycle, and the minimum learning rate is always 0.00003. Fig. 9 shows the adjustment of the learning rate with the number of iterations.

The aforementioned training strategy was applied to the CNN, and the average loss curve of the volume fraction for the six texture components over the course of the training process is illustrated in Fig. 10. As illustrated in the figure, the loss curves of the six texture components on the training set and the test set exhibit a convergence trend as the number of iterations increases. This convergence indicates that the model not only learns the general structure of the data set but also demonstrates the capacity to accurately predict each texture volume fraction.

[1] Mao Weimin and Zhang Xinming. *Quantitative Texture Analysis of Crystalline Materials*. Metallurgical Industry Press, 1993.

[2] H-R Wenk and P Van Houtte. Texture and anisotropy. *Rep. Prog. Phys.*, 67:1367, 2004.

[3] Olaf Engler and Valerie Randle. Introduction to texture analysis: Macrotexture, microtexture, and orientation mapping, 2000.

[4] LIU Yun-tao et al. Neutron nondestructive techniques and applications on failure analysis. *Failure Analysis and Prevention*, 16(1):70–75, 82, 2021.

[5] A. J. Wilkinson and T. B. Britton. Strains, planes, and ebsd in materials science. *Materials today*, 15(9):366–376, 2012.

[6] Saeed Moemeni and Kamran Dehghani. An investigation to microstructural and texture evolution during the cold rolling of al0. 3cocrfeni high entropy alloy. *Materials Today Communications*, 40:109654, 2024.

[7] Yu-Qing Li et al. Microstructure analysis and bulk texture study in wide magnesium alloy sheets processed by twin-roll casting. *Advanced Materials*, 13:1771–1780, 2021.

[8] Guijie Zhu et al. The latest progress on neutron texture diffractometer at china advanced research reactor. *Nuclear Instruments and Methods in Physics Research Section A: Accelerators, Spectrometers, Detectors and Associated Equipment*, 1047:167729, 2023.

[9] Guijie ZHU et al. Data analysis and processing method for two-dimensional position sensitive detector of neutron texture diffractometer at china advanced research reactor. *Atomic Energy Science and Technology*, 57(4):857, 2023.

[10] Yiqing Hao et al. Machine-learning-assisted automation of

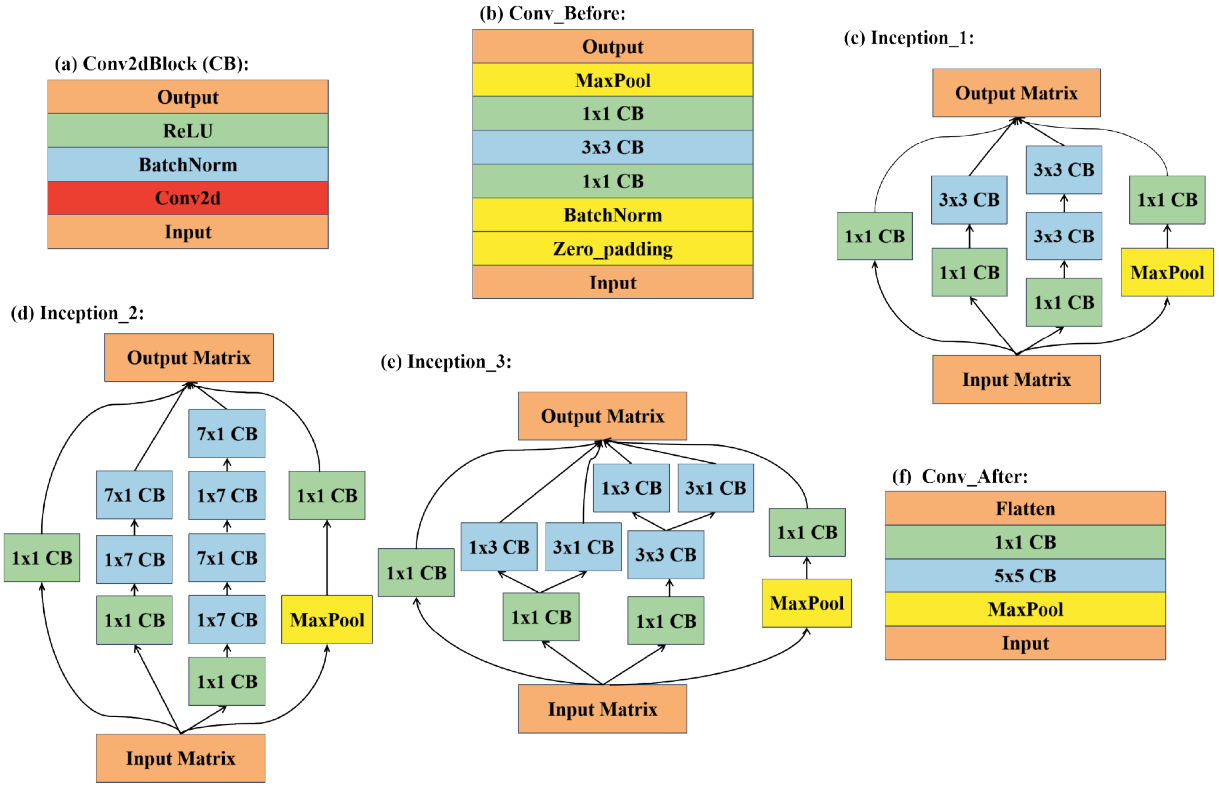

Fig. 8. The internal architecture of CNN.

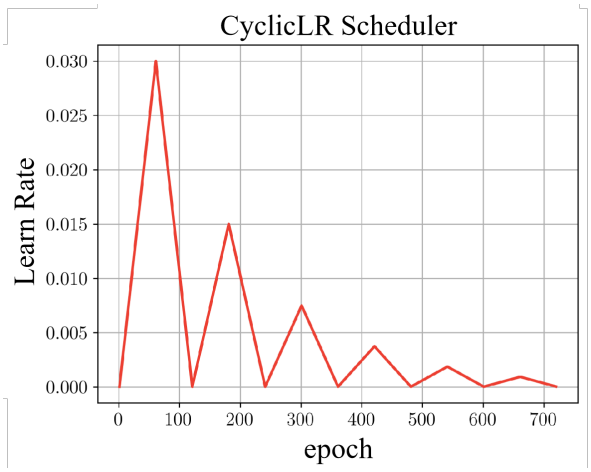

Fig. 9. CyclicLR learning rate scheduling strategy.

single-crystal neutron diffraction. *Journal of Applied Crystallography*, 56(2):519–525, 2023.

[11] Brendan Sullivan et al. Braggnet: integrating bragg peaks using neural networks. *Journal of Applied Crystallography*, 52(4):854–863, 2019.

[12] Mathieu Doucet et al. Machine learning for neutron reflectometry data analysis of two-layer thin films. *Machine Learning: Science and Technology*, 2(3):035001, 2021.

[13] Daniil Mironov et al. Towards automated analysis for neutron reflectivity. *Machine Learning: Science and Technology*, 2(3):035006, 2021.

[14] Singanallur V Venkatakrishnan et al. Adaptive sampling for accelerating neutron diffraction-based strain mapping. *Machine Learning: Science and Technology*, 4(2):025001, 2023.

[15] Guanghan Song et al. Deep learning methods on neutron scattering data. In *EPJ Web of Conferences*, volume 225, page 01004. EDP Sciences, 2020.

[16] José Ignacio Robledo et al. Learning from virtual experiments to assist users of small angle neutron scattering in model selection. *Scientific reports*, 14(1):14996, 2024.

[17] Davide Micieli et al. Accelerating neutron tomography experiments through artificial neural network based reconstruction. *Scientific Reports*, 9(1):2450, 2019.

[18] Adam Paszke et al. Automatic differentiation in pytorch. *NIPS*, 2017.

[19] Sergey Ioffe. Batch normalization: Accelerating deep network training by reducing internal covariate shift. *arXiv preprint arXiv:1502.03167*, 2015.

[20] Christian Szegedy et al. Rethinking the inception architecture for computer vision. In *Proceedings of the IEEE conference on computer vision and pattern recognition*, pages 2818–2826, 2016.

[21] Juan Tian, Ying-Xiang Li, and Tong-Yan Li. Contrastive study of activation function in convolutional neural network. *CSA*, 27(7):43–49, 2018.

[22] Leslie N Smith. Cyclical learning rates for training neural networks. In *2017 IEEE winter conference on applications of computer vision (WACV)*, pages 464–472. IEEE, 2017.

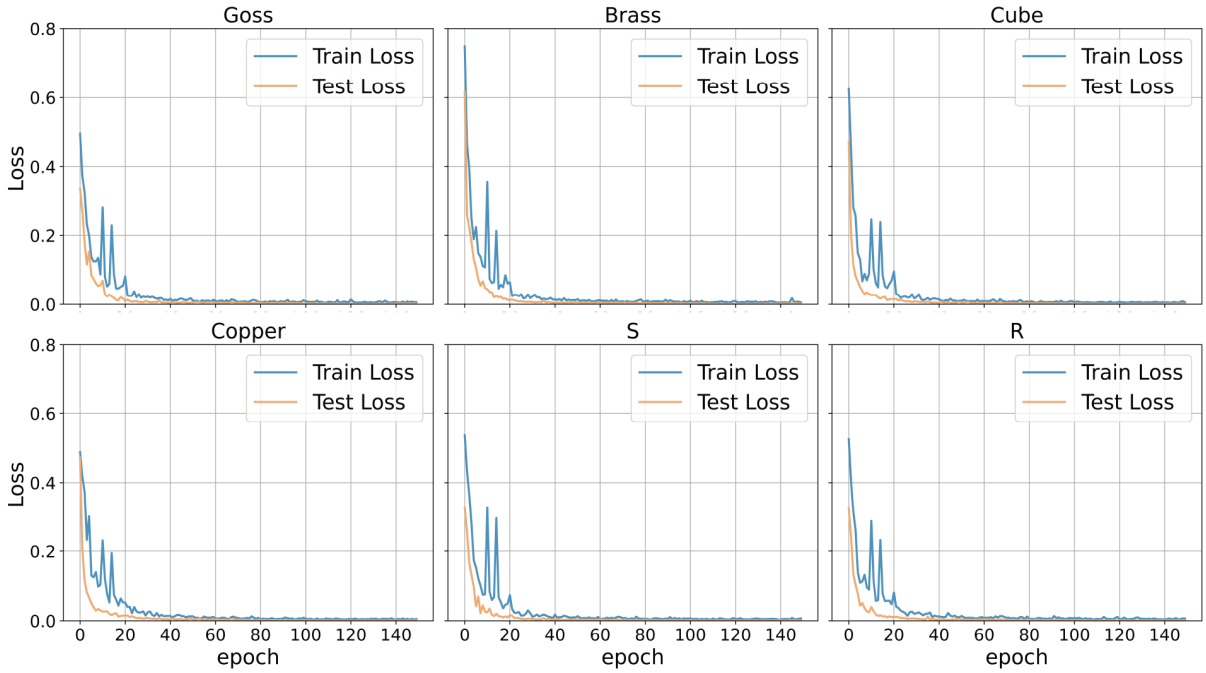

Fig. 10. The loss function change curve of six texture volume fraction prediction.